



ORIGINAL ARTICLE

The IGS contribution to ITRF2014

Paul Rebischung¹ · Zuheir Altamimi¹ · Jim Ray² · Bruno Garayt³

Received: 19 October 2015 / Accepted: 11 March 2016 / Published online: 8 April 2016
© Springer-Verlag Berlin Heidelberg 2016

Abstract Following the first reprocessing campaign performed by the International GNSS Service (IGS) in 2008, a second reprocessing campaign (repro2) was finalized in 2015. Nine different Analysis Centers (ACs) reanalyzed the history of GNSS data collected by a global tracking network back to 1994 using the latest available models and methodology, and provided daily terrestrial frame solutions among other products. Daily combinations of the AC terrestrial frame solutions provided the IGS input to the next release of the International Terrestrial Reference Frame (ITRF2014). From weighted root mean squares values of the residuals of the daily repro2 combinations, the overall inter-AC level of agreement is assessed to be 1.5 mm for the horizontal components and 4 mm for the vertical component of station positions, 25–40 μas for pole coordinates, 140–200 $\mu\text{as/day}$ for pole rates, 8–20 $\mu\text{s/day}$ for calibrated length-of-day estimates, 4 mm for the X and Y components of geocenter motion, 8 mm for its Z component and 0.5 mm for the terrestrial scale. On the long term, the origins (resp. scales) of the AC terrestrial frames show relative offsets and rates within ± 3 mm and ± 0.3 mm/year (resp. ± 0.5 mm and

± 0.05 mm/year). The combination residuals also present AC-specific features, some of which are explained by known analysis specifics, while others remain under investigation.

Keywords IGS · GNSS · Reprocessing · ITRF · Terrestrial reference frame · Combination

1 Introduction

Following the first successful reprocessing campaign (repro1; Steigenberger et al. 2006, 2009; Collilieux et al. 2011) performed by the International GNSS Service (IGS; Dow et al. 2009) in 2008, a second IGS reprocessing campaign (repro2) was recently undertaken. GNSS data collected by a global tracking network from 1994 to 2014 were reanalyzed by different Analysis Centers (ACs) using the latest available models and methodology. Besides supplying an improved consistent set of GNSS geodetic products, one major goal of the repro2 campaign was to provide the IGS input to the next release of the International Terrestrial Reference Frame (ITRF2014), in the same way as the repro1 campaign provided the IGS input to ITRF2008 (Altamimi et al. 2011).

A complete list of the models and conventions used in the repro2 data analyses can be found at <http://acc.igs.org/reprocess2.html>, where individual modeling aspects that have been changed since the repro1 campaign, are new, or have not been widely adopted previously have been highlighted using red font. The main updates since the repro1 campaign are:

- a switch from weekly to daily terrestrial frame integrations made to facilitate the study of station displacements (Griffiths and Choi 2013; Rebischung et al. 2013, IGSMail-6613),

J. Ray: Retired.

Electronic supplementary material The online version of this article (doi:[10.1007/s00190-016-0897-6](https://doi.org/10.1007/s00190-016-0897-6)) contains supplementary material, which is available to authorized users.

✉ Paul Rebischung
paul.rebischung@ign.fr

¹ IGN LAREG, Univ Paris Diderot, Sorbonne Paris Cité,
5 rue Thomas Mann, 75205 Paris Cedex 13, France

² National Oceanic and Atmospheric Administration, National
Geodetic Survey, Silver Spring, Maryland, USA

³ IGN SGN, 73 avenue de Paris, 94165 Saint-Mandé Cedex,
France

- the analysis, by some ACs, of GLONASS data in addition to GPS data,
- the implementation of the IGb08/igs08.atx reference frame and calibration framework (Rebischung et al. 2012, IGSMAIL-6354, IGSMAIL-6663),
- the implementation, mostly, of the IERS 2010 Conventions (Petit and Luzum 2010), regarding in particular the conventional mean pole model, the geopotential model, tidal station displacements, tidal variations in the Earth's rotation, tropospheric and ionospheric propagation delays,
- the implementation, partly, of new attitude models for eclipsing satellites (Kouba 2009; Dilssner 2010; Dilssner et al. 2011),
- the modeling of Earth radiation pressure (Rodriguez-Solano et al. 2011a,b) and, mostly, of antenna thrust (<http://acc.igs.org/orbits/thrust-power.txt>) acting on satellites.

Table 1 lists the AC contributions consistent with the repro2 standards that were available by the end of February 2015 (deadline for providing the IGS contribution to ITRF2014). The complete contributions of most ACs comprise a dedicated set of reprocessed products followed by consistent operational products (see column “Product acronyms and time spans”). The column “Remarks” indicates some AC specifics and main departures from the repro2 standards. The products delivered by the ACs include satellite orbits and clocks as well as daily terrestrial frame solutions in the form of SINEX files. In addition to the daily “cf2” products, COD also provided a series of 3-day solutions named

“co2”. The “co2” solutions were not considered in this work because of their departure from the repro2 specification for daily data integrations, but they will be used in a future study of the impact of orbital arc length on GNSS station position time series.

To perform an inter-AC comparison and form a weighted combined product set that can potentially maximize the benefits from the AC solutions while minimizing their weaknesses, the daily AC SINEX solutions were combined. Preliminary combinations revealed a number of quality issues and systematic errors in the initial contributions of several ACs. Most of the concerned ACs were able to submit corrected products in time. But a few remaining issues led to assigning zero weights or pre-eliminate specific parameters from certain AC solutions in the final combinations (Table 2). The final repro2 daily combined SINEX solutions, named “ig2”, were made available on February 27, 2015 (IGSMAIL-7055) and can be retrieved from the IGS data centers (<http://igs.org/about/data-centers>). They cover the period from 1994-01-02 to 2015-02-14 (GPS weeks 730–1831) and constitute the IGS input to ITRF2014.

Section 1 of this article aims at describing the methodology used for the daily repro2 SINEX combinations. The residuals from the daily combinations are then discussed in Sect. 2. Section 3 finally covers some aspects of the repro2 combined dataset.

From 1999 to 2010, combinations of the weekly AC SINEX solutions were performed at Natural Resources Canada with the methodology described in Ferland et al. (2000). The SINEX combinations were then taken on by the Institut National de l'Information Géographique et Forestière

Table 1 AC contributions to the repro2 campaign

AC	Institution	Product acronyms and time spans	Remarks
COD	Center for Orbit Determination in Europe	cf2: 1994-01-02 to 2013-12-28 cof: 2013-12-29 to 2015-02-14	GLONASS data included starting from 2002
EMR	Natural Resources Canada	em2: 1994-10-02 to 2014-03-29 emr: 2014-03-30 to 2015-02-14	
ESA	European Space Operations Center	es2: 1995-01-01 to 2014-04-19 esa: 2014-04-20 to 2015-02-14	GLONASS data included starting from 2009
GFZ	GeoForschungsZentrum	gf2: 1994-01-02 to 2015-01-17 gfz: 2015-01-18 to 2015-02-14	2nd order ionospheric corrections not applied
GRG	Groupe de Recherche en Géodésie Spatiale	gr2: 1998-01-01 to 2014-12-31 grg: 2015-01-01 to 2015-02-14	GLONASS data included starting from 2009
JPL	Jet Propulsion Laboratory	jp2: 1994-01-02 to 2014-10-25 jpl: 2014-10-26 to 2015-02-14	30-h data integrations
MIT	Massachusetts Institute of Technology	mi2: 1994-01-02 to 2014-08-02 mit: 2014-08-03 to 2015-02-14	
GTZ	GeoForschungsZentrum	gt2: 1994-01-02 to 2012-12-29	GFZ contribution to the IGS TIGA project
ULR	Université de la Rochelle	ul2: 1995-01-01 to 2014-12-31	Contribution to the IGS TIGA project

Table 2 Actions taken to exclude specific AC contributions from the final repro2 combinations

AC	Time period	Action	Reason
GFZ	1994-01-01 to 2012-12-29	Zero weight assigned	Redundancy with the GTZ solutions
GRG	Whole repro2 period	Zero weight assigned	Large station position residuals (Sect. 2.1)
ULR	Whole repro2 period	Geocenter coordinates pre-eliminated	Large geocenter residuals (Sect. 2.3)
ULR	2013-12-31 to 2014-12-31	Zero weight assigned	Large scale offsets (Sect. 2.4)

(IGN) with a slightly different combination methodology briefly described in [Rebischung and Garayt \(2013\)](#). Several changes have since then been brought to the SINEX combination process, for instance upon the switch from weekly to daily terrestrial frame integrations, but have so far remained largely undocumented. The main goal of this section is, therefore, to give a detailed description of the latest SINEX combination methodology employed at IGN. The process described in this section was used for the daily repro2 SINEX combinations and has been used for the daily operational IGS SINEX combinations since GPS week 1832 (2015-02-15).

Table 3 lists the official products from the daily operational IGS SINEX combinations, available at the IGS global data centers, which will be referred to in the following. The products from the daily repro2 SINEX combinations have the same denomination except that they use the prefix “ig2” instead of “igs”.

1.1 Input data

Each daily analysis performed by an IGS AC consists in adjusting a vector of parameters \mathbf{x} to a set of code and phase observations acquired by ground GNSS stations. Such an adjustment leads to a normal equation:

$$\mathbf{N}(\mathbf{x} - \mathbf{x}_0) = \mathbf{b} \quad (1)$$

where \mathbf{x}_0 is a vector of a priori parameter values. It is possible to pre-eliminate specific parameters from such a normal equation so as to retain a subset of parameters of interest only. Before providing their SINEX solutions, the ACs thus pre-eliminate all estimated parameters but station coordinates, Earth rotation parameters (ERPs), possibly satellite phase center offsets (PCOs), and geocenter coordinates in the case of COD, so that we will now consider that \mathbf{x} contains those parameters only. The provided ERPs are the pole coordinates at noon (x_p, y_p), the rates of change of the pole coordinates (\dot{x}_p, \dot{y}_p), the UT1–UTC offset at noon (constrained to some a priori value) and the excess length-of-day (LOD).

GNSS observations do not provide enough information to unambiguously estimate station coordinates and ERPs. This

Table 3 Official products from the daily operational IGS SINEX combinations. yy stands for the 2-digit year, wwww for the GPS week and d for the day of week (0–6)

File	Description
igsyyPwwwd_all.snx	Daily combined solution (all stations)
igsyyPwwwd_all.ssc	Daily combined solution without covariance matrix (all stations)
igsyyPwwwd.snx	Daily combined solution (stations with DOMES numbers only)
igsyyPwwwd.ssc	Daily combined solution without covariance matrix (stations with DOMES numbers only)
igsyyPwwwd.res	Residuals between daily AC solutions and daily combined solution
igsyyPwwwd_IGS.res	Residuals between daily AC solutions and IGS cumulative solution
igsyyPwwwd_ITR.res	Residuals between daily AC solutions and IGS reference frame
igsyyPwww.erp	ERPs Extracted from the daily combined solutions
igsyyPwww.sum	SINEX combination summary

translates to the fact that the normal matrix \mathbf{N} has three orientation singularities so that the normal equation has an infinite number of solutions. To obtain a unique solution from the normal equation, but also to practically fix specific parameters like satellite PCOs, the ACs consequently impose additional constraints to the estimated parameters. Provided that these constraints are applied as pseudo-observations with respect to the a priori parameters \mathbf{x}_0 , the resulting constrained normal equation can be written:

$$(\mathbf{N} + \mathbf{N}_c)(\mathbf{x} - \mathbf{x}_0) = \mathbf{b} \quad (2)$$

where \mathbf{N}_c is the normal matrix of constraints and $\mathbf{N} + \mathbf{N}_c$ is invertible. Such a constrained normal equation leads to a unique solution:

$$\hat{\mathbf{x}} = \mathbf{x}_0 + (\mathbf{N} + \mathbf{N}_c)^{-1} \mathbf{b}. \quad (3)$$

The covariance matrix associated with the estimated parameters $\hat{\mathbf{x}}$ is:

$$\mathbf{Q}_{\hat{\mathbf{x}}} = (\mathbf{N} + \mathbf{N}_c)^{-1}. \quad (4)$$

In their daily SINEX files, all ACs provide the a priori and estimated parameters \mathbf{x}_0 and $\hat{\mathbf{x}}$. Some readily provide the original non-constrained normal equation, i.e. \mathbf{N} and \mathbf{b} . The others provide the covariance matrix of the estimated parameters $\mathbf{Q}_{\hat{\mathbf{x}}}$, together with (sometimes partial; see Sect. 1.2) information about the applied constraints, i.e. \mathbf{N}_c or $\mathbf{Q}_c = \mathbf{N}_c^{-1}$.

1.2 Preprocessing

A number of operations are applied to the daily AC SINEX solutions before they are combined. This section describes the succession of those preprocessing steps.

Estimation of AC \rightarrow IGb08 transformation parameters
Before any further operation, the seven parameters of a similarity transformation are estimated between the terrestrial frame solution $\hat{\mathbf{x}}$ of each AC and the IGb08 reference frame (Rebischung et al. 2012, IGSMAIL-6663). These parameters are reported in Sect. 5-3 of each combination summary, with the main purpose of providing the rotations to be applied to the AC orbits during the IGS final orbit combination to maintain full product consistency.

An identity weight matrix and only a subset of stations are used for the estimation of the seven transformation parameters. Stations of the IGb08 *core* network (Rebischung et al. 2012, IGSMAIL-6663) with valid coordinates at the combination epoch are first retained. From this selection, stations with abnormally large 3D formal errors in the AC solution (i.e. larger than twice the median of the 3D formal errors) are then rejected. An iterative screening of the transformation residuals is finally performed to reject possible outliers. At each step, any station with a residual larger than three times the RMS of the residuals in either the East, North or Up component is rejected.

Unconstraining For AC contributions provided as constrained solutions, the next step consists in recovering the original non-constrained normal equation. In these cases, the right-hand side of the normal equation is first recovered by:

$$\mathbf{b} = \mathbf{Q}_{\hat{\mathbf{x}}}^{-1}(\hat{\mathbf{x}} - \mathbf{x}_0). \quad (5)$$

The information reported in the MATRIX/APRIORI and/or SOLUTION/APRIORI blocks of the SINEX file is then used

to build the normal matrix of the *reported* constraints \mathbf{N}_c^r , and a *partially* unconstrained normal matrix is obtained by:

$$\mathbf{N}^p = \mathbf{Q}_{\hat{\mathbf{x}}}^{-1} - \mathbf{N}_c^r. \quad (6)$$

We fix at this stage a certain number of parameters to their a priori values by removing the corresponding lines and columns from \mathbf{N}^p and \mathbf{b} . This stage is performed for all AC contributions including those provided as normal equations. The fixed parameters include the UT1–UTC offset (not estimable from GNSS observations), the satellite PCOs (henceforth considered fixed to their igs08.atx values) and the geocenter coordinates present in COD’s normal equations.

In case where all the applied constraints are reported in the SINEX file ($\mathbf{N}_c^r = \mathbf{N}_c$), then \mathbf{N}^p is nothing but the original non-constrained normal matrix \mathbf{N} . In the cases of several ACs, however, \mathbf{N}^p does not show the three expected orientation singularities of \mathbf{N} . In those cases, we make the assumption that the remaining unreported constraints correspond to minimal no-net-rotation constraints and recover \mathbf{N} by:

$$\mathbf{N} = \mathbf{N}^p - \mathbf{N}^p \mathbf{K} (\mathbf{K}^T \mathbf{N}^p \mathbf{K})^{-1} \mathbf{K}^T \mathbf{N}^p \quad (7)$$

where \mathbf{K} denotes a matrix whose columns form a basis of $\text{Ker}(\mathbf{N})$, i.e. correspond to three rotations of the station network plus consistent variations of the pole coordinates. A proof of Eq. 7 can be found in Sect. B.2.4 of Rebischung (2014).

Ocean pole tide corrections Although recommended by the IERS 2010 Conventions, the correction of station displacements caused by ocean pole tide (OPT) was not made by all ACs in their repro2 analyses. Since the OPT displacements have mostly annual and Chandler periods, their effect on station positions can be corrected as efficiently at the level of daily solutions (or normal equations) as during the data analysis. To reach the best possible consistency, we, therefore, applied OPT corrections to the unconstrained normal equations of the non-compliant ACs (COD, ESA, MIT and ULR). These corrections are concretely applied by gathering the OPT station displacements into a vector $\delta\mathbf{x}_{OPT}$ and modifying the right-hand side of the normal equation by:

$$\mathbf{b} \leftarrow \mathbf{b} - \mathbf{N} \delta\mathbf{x}_{OPT}. \quad (8)$$

LOD calibration GNSS-derived LOD estimates are known to be affected by significant time- and AC-dependent biases (Ray 1996, 2009). These biases have been handled in the same pragmatic way since the beginning of the IGS SINEX combinations: each daily AC LOD estimate is corrected for a bias computed as the mean difference, over the n previous days, between the AC LOD estimates and the LOD values reported in the IERS Bulletin A. While a 21-day sliding window was previously used for these calibrations, it was

changed to a 10-day window in the repro2 SINEX combinations and in the operational SINEX combinations since GPS week 1832, to become consistent with the AC LOD calibrations applied during the IGS orbit and clock combinations. The AC LOD calibrations are concretely made by modifying the right-hand side of the AC unconstrained normal equations in a similar way as in Eq. 8.

Making geocenter coordinates explicit Since GNSS satellites orbit around the Earth's center of mass (CM), the station positions implied by the AC normal equations refer in theory to CM-centered frames. However, significant biases exist between the origins of the AC solutions (Collilieux et al. 2011; Rebischung 2014; Sect. 2.3), owing to the weak sensitivity of global GNSS solutions to the location of CM combined with orbit modeling deficiencies (Meindl et al. 2013; Rebischung et al. 2014).

To avoid that the large inter-AC origin biases leak into the station position residuals from the combination, a two-step combination procedure had been developed by Rebischung and Garayt (2013), where inter-AC translation parameters were first estimated and then fixed in a final combination. In the repro2 SINEX combinations and in the operational SINEX combinations since GPS week 1832, a more rigorous approach has been implemented, where geocenter coordinates are made explicit in each AC solution. The unconstrained normal equation of each AC is concretely re-parameterized through the following variable change:

$$\mathbf{x}_i^{\text{CM}} = \mathbf{x}_i^{\text{RF}} - \mathbf{x}_{\text{CM}}^{\text{RF}} \quad \text{for all station } i \quad (9)$$

where \mathbf{x}_i^{CM} are the original coordinates of station i (referred to the observed, biased CM), \mathbf{x}_i^{RF} are the re-parameterized coordinates of station i (referred to a given reference frame, e.g. IGB08) and $\mathbf{x}_{\text{CM}}^{\text{RF}}$ are the coordinates of the observed CM in the same reference frame, i.e. the observed geocenter coordinates. This re-parameterization allows the AC geocenter coordinates to be combined separately from the station coordinates, so that the inter-AC origin biases are reflected by the geocenter residuals from the combination rather than as part of the station position residuals.

Parameter pre-elimination Before their inversion, specific parameters may finally be pre-eliminated from the AC normal equations, so that they will not contribute to the combination. In the repro2 combinations, AC ERP estimates were all retained. Geocenter coordinates were pre-eliminated from ULR's normal equations due to abnormally large offsets compared to the other ACs (see Sect. 2.3). The coordinates of some stations (listed in Sect. 4 of the combination summaries) were finally pre-eliminated from specific AC solutions due to either exceptionally large coordinate differences with the other ACs, or metadata errors (wrong antenna and/or eccentricity). 231,249 daily AC station position estimates were

thus rejected out of 12,867,344 (i.e. 1.8 %). By means of such pre-eliminations, it was in particular ensured that, over the whole set of repro2 combinations, all ACs contributing to the same station on the same day reported the same antenna and eccentricity.

Inversion The preprocessed AC normal equations are then solved. Since geocenter coordinates were explicit, the pre-processed AC normal matrices have not only three orientation singularities, but also three origin singularities. A minimal set of six no-net-rotation (NNR) and no-net translation (NNT) constraints are, therefore, added to the AC normal matrices before their inversion. These constraints are applied with respect to the IGB08 reference frame, using the same set of core stations as for the estimation of the AC \rightarrow IGB08 transformation parameters. We obtain at this step a preprocessed solution for each AC, i.e. estimates of station positions, geocenter coordinates and ERPs, together with the associated covariance matrix \mathbf{Q} .

A priori scaling Each AC covariance matrix is finally scaled by an a priori variance factor: $\mathbf{Q} \leftarrow \sigma^2 \mathbf{Q}$. This factor is obtained from the median $\bar{\sigma}_{3D}$ (expressed in mm) of the 3D station position formal errors in the preprocessed AC solution by:

$$\sigma^2 = (4/\bar{\sigma}_{3D})^2. \quad (10)$$

This scaling comes down to setting the median 3D station position formal error to 4 mm in all AC solutions, which ensures a balance between the AC contributions in the first iterations of the combination. The value of 4 mm was chosen so that the a posteriori variance factors applied for the final combination (Sect. 1.4) are close to unity.

1.3 Iterative combinations

Once all AC solutions have been pre-processed, those contributing to the combined solution (i.e. with non-zero weights) are iteratively combined and checked for outliers. The combination consists in a standard weighted least-squares adjustment where the parameters from the preprocessed AC solutions are taken as observations. The combination model is given by the following equations, adapted from Altamimi et al. (2007):

$$\left\{ \begin{array}{l} \mathbf{x}_i^s = \mathbf{x}_i^c + \mathbf{t}^s + \mathbf{R}^s \mathbf{x}_i^c + \mathbf{v}_i^s \\ \mathbf{x}_{\text{CM}}^s = \mathbf{x}_{\text{CM}}^c + \mathbf{t}^s + \mathbf{v}_{\text{CM}}^s \\ x_p^s = x_p^c + r_Y^s + v_{x_p}^s \\ y_p^s = y_p^c + r_X^s + v_{y_p}^s \\ \dot{x}_p^s = \dot{x}_p^c + v_{\dot{x}_p}^s \\ \dot{y}_p^s = \dot{y}_p^c + v_{\dot{y}_p}^s \\ \text{LOD}^s = \text{LOD}^c + v_{\text{LOD}}^s \end{array} \right. \quad (11)$$

where

- $\mathbf{x}_i^s, \mathbf{x}_{CM}^s, x_p^s, y_p^s, \dot{x}_p^s, \dot{y}_p^s$ and LOD^s denote, respectively, the coordinates of some station i , the geocenter coordinates and the ERPs in the preprocessed solution of AC s ,
- $\mathbf{x}_i^c, \mathbf{x}_{CM}^c, x_p^c, y_p^c, \dot{x}_p^c, \dot{y}_p^c$ and LOD^c denote the corresponding parameters in the combined solution,
- $\mathbf{t}^s = [t_X^s, t_Y^s, t_Z^s]^T$ is a vector of translations estimated between the terrestrial frame of AC s and the combined terrestrial frame,
- $\mathbf{R}^s = \begin{bmatrix} 0 & -r_Z^s & r_Y^s \\ r_Z^s & 0 & -r_X^s \\ -r_Y^s & r_X^s & 0 \end{bmatrix}$ is a matrix composed of rotation angles estimated between the terrestrial frame of AC s and the combined terrestrial frame,
- $\mathbf{v}_i^s, \mathbf{v}_{CM}^s, v_{x_p}^s, v_{y_p}^s, v_{\dot{x}_p}^s, v_{\dot{y}_p}^s$ and v_{LOD}^s are the combination residuals of AC s .

Equation 11 can be written in a more condensed way as:

$$\mathbf{x}^s = \mathbf{A}^s \mathbf{x}^c + \mathbf{v}^s \quad (12)$$

where \mathbf{x}^s is a vector containing all parameters in the preprocessed solution of AC s , \mathbf{A}^s is the design matrix of AC s , \mathbf{x}^c is a vector containing all estimated parameters (i.e. the combined station positions, geocenter coordinates and ERPs, as well as the translation and rotation parameters) and \mathbf{v}^s is a vector containing the combination residuals of AC s . The weight matrix used for the combination is block diagonal, its blocks being the inverses of the preprocessed, scaled AC covariance matrices, i.e. $\mathbf{P}^s = (\mathbf{Q}^s)^{-1}$.

Translations and rotations are estimated between the terrestrial frame of each AC and the combined terrestrial frame to discard the arbitrary information stemming from the NNT and NNR constraints applied during the preprocessing step. On the other hand, no scale factors are estimated between the AC frames and the combined frame. The scales of the AC frames are indeed conventionally defined by the igs08.atx satellite PCO values (Zhu et al. 2003; Ray et al. 2013b) and actually show an excellent agreement (see Sect. 2.4). Moreover, the estimation of AC scale factors during the combination would require constraining the scale of the combined frame to that of some reference frame and it is known that such alignments in scale would remove part of the non-linear motions of the station network (e.g. loading deformations) from the daily combined frames, even if using a relatively uniform network of reference stations (Collilieux et al. 2012). Given the good consistency between the scales of the AC frames, we therefore chose not to estimate AC scale factors during the combination, so as to avoid such aliasing of the non-linear station motions.

The estimation of translation and rotation parameters results in six singularities in the combined normal equation, which are compensated by adding NNT and NNR constraints between the combined terrestrial frame and IGB08. On the other hand, no constraint is needed to define the scale of the combined frame, which is a natural mean of the AC frame scales, and hence conventionally defined by the igs08.atx satellite PCO values.

Solving the constrained combined normal equation leads to the adjusted parameter vector $\hat{\mathbf{x}}^c$, to the associated covariance matrix $\mathbf{Q}_{\hat{\mathbf{x}}^c}$ and to the AC residuals $\hat{\mathbf{v}}^s = \mathbf{x}^s - \mathbf{A}^s \hat{\mathbf{x}}^c$. At each iteration, the AC station position residuals are checked for outliers. The detection of outliers is based on AC- and component-specific thresholds. To define these thresholds, we start by computing the weighted root mean squares (WRMS) of the AC station position residuals along each East, North and Up component:

$$w_l^s = \sqrt{\sum_{i=1}^{n^s} \frac{(v_{i,l}^s)^2}{(\sigma_{i,l}^s)^2} / \sum_{i=1}^{n^s} \frac{1}{(\sigma_{i,l}^s)^2}} \quad (13)$$

where the subscript l stands for either East, North or Up, n^s is the number of stations in the solution of AC s , $v_{i,l}^s$ is the combination residual for station i , AC s and component l , and $\sigma_{i,l}^s$ is the corresponding formal error, extracted from the AC covariance matrix \mathbf{Q}^s .

However, as shown by Sillard (1999), such WRMS of the combination residuals gives biased estimates of the WRMS of the true AC station position errors. Based on the method proposed by Sillard (1999), we, therefore, compute unbiased estimates of the WRMS of the AC station position errors by:

$$w_l^{s,u} = \sqrt{\frac{n^s}{f_l^s} w_l^s} \quad (14)$$

where

$$f_l^s = n^s - \text{tr}(\mathbf{R}_l^s \mathbf{A}^s \mathbf{Q}_{\hat{\mathbf{x}}^c} (\mathbf{R}_l^s \mathbf{A}^s)^T (\mathbf{R}_l^s \mathbf{Q}^s (\mathbf{R}_l^s)^T)^{-1}) \quad (15)$$

and \mathbf{R}_l^s denotes the matrix mapping the full AC residual vector $\hat{\mathbf{v}}^s$ to the vector of station position residuals along component l . See Sect. 2.1 for a further discussion on the difference between those biased and unbiased WRMS.

The AC- and component-specific thresholds used to flag outliers are finally set to $5w_l^{s,u}$. More precisely, any station with a residual larger than $5w_l^{s,u}$ in either the East, North or Up component is first marked as a potential outlier in solution s . Then, each station marked as a potential outlier in the solutions of several ACs is kept as an effective outlier in only the AC solution with the largest 3D residual for this station. It is thus ensured one station cannot be rejected from more than one AC solution during the same iteration. The effective

outliers are then eliminated from the corresponding AC solutions and the combination is rerun. Iterations are performed until no outlier is detected anymore. Lists of the eliminated stations can be found in Sect. 5-7 of the combination summaries. 68,522 daily AC station position estimates were thus rejected out of 12,867,344 (i.e. 0.5 %).

1.4 Final combination

Once the AC solutions contributing to the combined solution have been cleaned for outliers, a final combination is performed. The only differences between this final combination and the previous iteration are that:

- a posteriori variance factors based on the residuals from the previous iteration are used to rescale the AC covariance matrices,
- the origin and orientation of the combined solution are defined through a specific set of available IGb08 core stations (instead of all available IGb08 stations).

A posteriori scaling The a posteriori variance factors (σ_f^s)² used for the final scaling of the AC covariance matrices are based on a variance component estimation method known as “degree of freedom estimation” (Sillard 1999). They are computed from the results of the previous iteration by:

$$(\sigma_f^s)^2 = \frac{(\hat{\mathbf{v}}^s)^T \mathbf{P}^s \hat{\mathbf{v}}^s}{n_{\text{par}}^s - \text{tr}(\mathbf{A}^s \mathbf{Q}_{\hat{\mathbf{x}}^c} (\mathbf{A}^s)^T \mathbf{P}^s)} \quad (16)$$

where n_{par}^s denotes the number of parameters in the solution of AC s .

Reference frame definition The origin and orientation of the final combined solution are still defined by NNT and NNR constraints with respect to IGb08. But to ensure an optimal alignment of the combined solution to IGb08, these constraints are applied to a subset only of the available core stations. The selection of those effective reference stations is done in exactly the same way as for the estimation of the AC → IGb08 transformation parameters (Sect. 1.2). Note that the applied constraints are reported in the MATRIX/APRIORI block of the combined SINEX files, so that they can be removed for specific uses.

1.5 Further comparisons

The AC solutions not contributing to the combination (i.e. with zero weights) are then compared to the final combined solution. These comparisons are based on Eq. 11, where the combined parameters are now fixed, so that only the three translation and three rotation parameters are estimated. The weight matrices used for the comparisons are the inverses

of the preprocessed AC covariance matrices. The residuals from either the final combination (for the contributing ACs) or the previous comparisons (for the non-contributing ACs) are reported in the daily residual files (igsyyPwwwd.res).

Similar comparisons are finally made between all AC solutions on one hand and IGb08 (resp. the IGS cumulative solution) on the other. The comparison residuals are reported in the igsyyPwwwd_ITR.res (resp. igsyyPwwwd_IGS.res) files.

2 Residuals from the daily repro2 combinations

The combination residuals $\hat{\mathbf{v}}^s$ indicate how well each daily AC solution agrees with the corresponding daily combined solution, or in other words, how the different AC solutions depart from their weighted mean. A thorough study of the daily repro2 combination residuals was, therefore, essential for several reasons. It first exposed serious quality issues and systematic errors in some of the initial AC repro2 contributions, most of which could be solved in time for the final repro2 combinations. It also allowed smaller systematic inter-AC differences to be seen, presumably linked with analysis specifics. It finally allowed an assessment of the level of agreement between the contributing ACs for the various combined parameters, thus giving indications of the internal precision of the AC products. Remember, however, that the inter-AC levels of agreement discussed in the following do not reflect the absolute accuracy of the AC products, since they do not account for the errors common to all ACs (i.e. induced by common modeling errors).

This section presents and discusses the residuals from the final daily repro2 combinations for station positions (Sect. 2.1), ERPs (Sect. 2.2) and geocenter coordinates (Sect. 2.3). Section 2.4 finally focuses on the agreement between the scales of the daily AC terrestrial frames.

2.1 Station position residuals

A global measure of the inter-AC level of agreement on station positions is given by the WRMS of the AC station position residuals. As mentioned in Sect. 1.3, the raw WRMS given by Eq. 13 are biased, and unbiased estimates of the WRMS of the true AC station position errors can be obtained by Eq. 14 for ACs contributing to the combination. Figure 1 shows smoothed time series of both the raw and unbiased WRMS of the AC station position residuals from the daily repro2 combinations, as well as of their ratios and of the number of stations present in the preprocessed daily AC solutions.

It can first be noted that, with a few exceptions, the WRMS time series of all ACs stay at comparable levels, meaning that the daily station position estimates provided by the different ACs are of quite homogeneous quality. The major exceptions

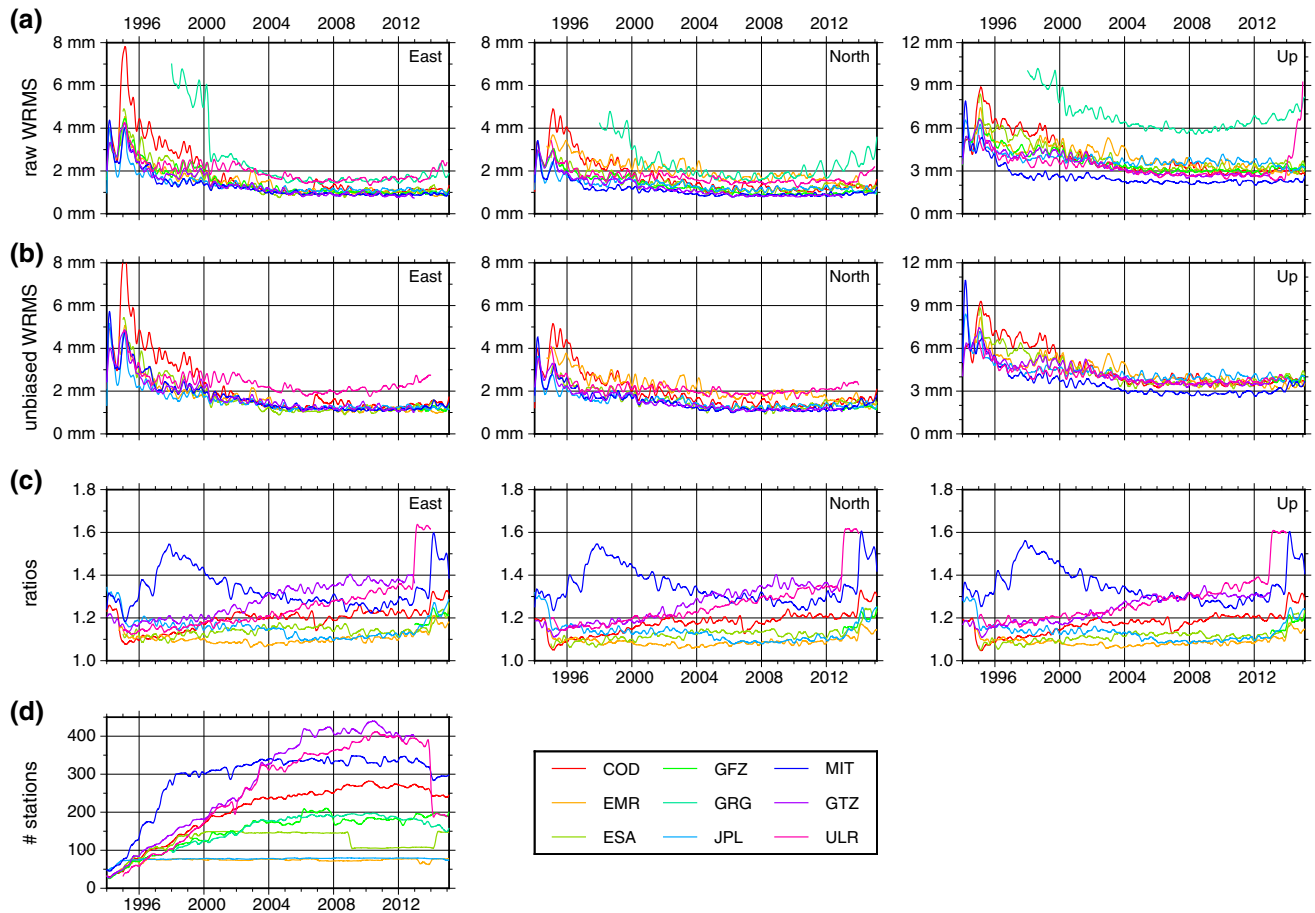


Fig. 1 From top to bottom: **a** time series of the raw WRMS (w_l^s from Eq. 13) of the AC station position residuals from the daily repro2 combinations; **b** time series of the unbiased WRMS ($w_l^{s,u}$ from Eq. 14; shown for the contributing ACs only); **c** time series of the ratios $w_l^{s,u}/w_l^s$

(shown for the contributing ACs only); **d** number of stations in the preprocessed daily AC solutions. For legibility, all time series were smoothed by a Vondrák filter (Vondrák 1969, 1977) with a 2.5 cpy cutoff frequency

that led to assigning zero weights to certain AC contributions are:

- The substantially larger WRMS of GRG's residuals in the Up component, and to a lesser degree in the North component. The cause of this deviation is still unknown and under investigation.
- The abnormal increase of the WRMS of ULR's residuals over year 2014 in the Up component (see Sect. 2.4).

Smaller deviations from the majority behavior can additionally be observed:

- The WRMS of ULR's residuals constantly stay above the average level in the East and North components after 1999, likely due to a sub-optimal combination of the station clusters used to form the full daily ULR solutions (Alvaro Santamaría-Gómez, personal communication). This also translates to a higher level of white noise in the time series of ULR's horizontal station position residual time series (see Fig. 2).

- The WRMS of COD's residuals are distinctly above the average level prior to 1999, especially in the East component, likely due to phase ambiguity fixing issues.
- The WRMS of EMR's residuals are constantly slightly above the average level in the North component. This seems to be due to small station-specific constant biases, but requires confirmation and further investigation.

It can also be noted that the *raw* WRMS of MIT's residuals are generally slightly below the average level, more markedly in the Up component. This could suggest that MIT's daily solutions are of better quality and hence dominate the daily combined solutions. However, the predominance of MIT is less marked in the *unbiased* WRMS time series, especially during years 1997–1999. During this period, MIT's solutions count much more stations than the other ACs, many of them being part of no other AC solution. Those stations processed by MIT only have almost zero residuals in the daily combinations and consequently drag down the *raw* WRMS of MIT's residuals. This effect is supposed to be corrected

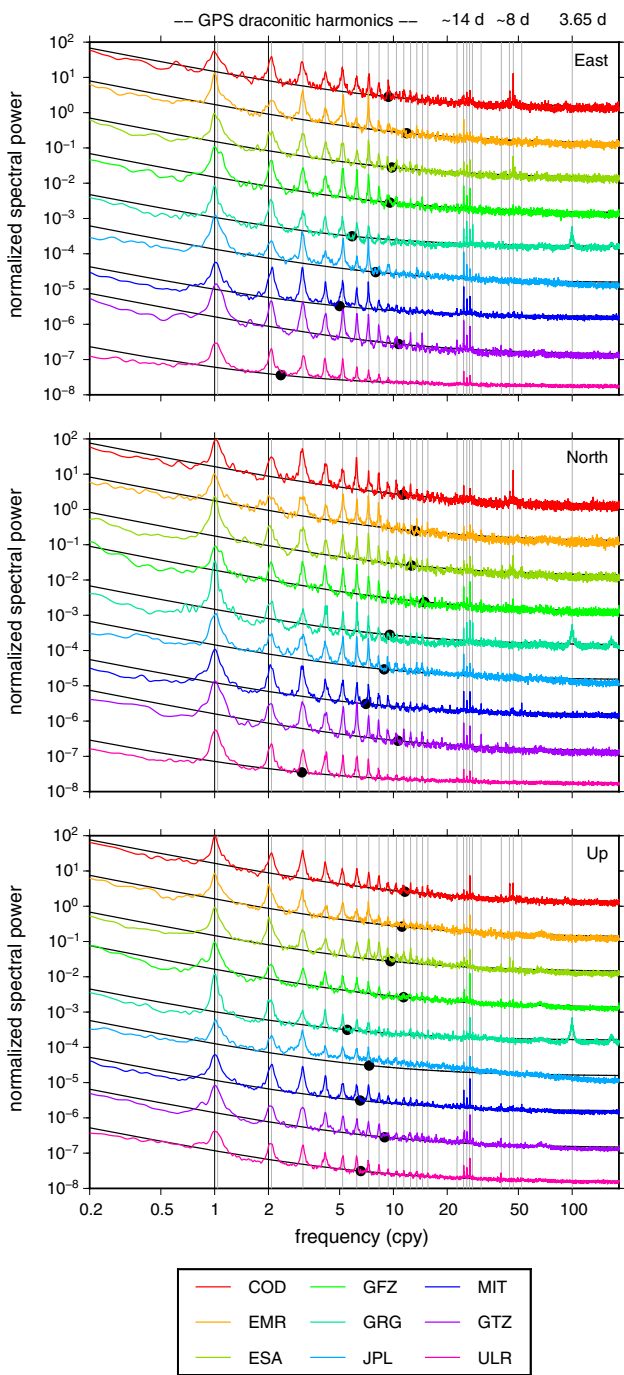


Fig. 2 Color lines averaged normalized Lomb–Scargle periodograms of the AC station position residual time series obtained as described in the text and offset by powers of 10 for clarity. *Black lines* results from the fits of white + flicker noise models (i.e. $a + b/f$ functions) to the averaged periodograms. The *black dots* indicate the crossover frequencies $f_0 = b/a$ where the estimated white and flicker noises have equal power. The *vertical black lines* indicate the 1 and 2 cpy frequencies. The *vertical gray lines* indicate the first 15 harmonics of the GPS draconitic year (1.04 cpy), several relevant periods around the fortnightly band (16.1, 14.8, 14.2, 13.7, 13.2 and 11.8 days), around the 8-day band (9.1, 8.2, 7.8 and 7.0 days) and the 3.65-day period

in the unbiased WRMS, which account for the redundancy between the AC station networks. But one cannot exclude that MIT's unbiased WRMS are still partly dragged down by those non-common stations. Moreover, it can be observed that starting from 2014 (when ULR's solutions do not contribute to the combinations anymore), the vertical unbiased WRMS of MIT's residuals get closer to the average level. Part of the apparent domination of MIT until 2013 might, therefore, also be related to the presence in the daily combinations of ULR's solutions, obtained with the same software as MIT's solutions.

Apart from those deviations, the unbiased WRMS time series of the different ACs show similar time evolutions, and stay practically constant starting from 2004, i.e. when the AC GPS station networks reach maturity. From 2004 onwards, the inter-AC level of agreement on station positions is at the level of about 1.5 mm in both horizontal components and 4 mm in the vertical component. Once again, these numbers give an indication of the internal precision of the daily AC station position estimates, but not of their absolute accuracy.

To gain insight into their spectral characteristics, time series of the station position residuals from the daily repro2 combinations were formed for each AC, station and East, North, Up component. Normalized Lomb–Scargle periodograms (Scargle 1982; Press et al. 1996) were computed for all series with at least 1000 data points over a common set of frequencies, and algebraically averaged for each AC and component. Figure 2 shows the resulting averaged normalized periodograms. Since normalized periodograms are shown, their absolute values cannot be interpreted, nor can the differences in magnitude between the AC periodograms. The only relevant information in Fig. 2 is the *shape* of the periodograms (including background continuum and sharp spectral features), as well as the differences in shape between the AC periodograms.

It can first be noted that the background noise present in the AC station position residual time series is generally well described by the sum of white and flicker noises. For almost all ACs and components, the crossover frequencies between the white and flicker noises are located between 5 and 15 cpy. The only exceptions concern the East and North components of ULR's residuals, which show noticeably lower crossover frequencies (2.3 and 3.1 cpy respectively), hence noticeably flatter periodograms. Though it cannot be definitely inferred from the normalized periodograms shown in Fig. 2, we think that this is due to a higher level of white noise in ULR's horizontal station position residual time series, since this would also explain the higher WRMS of ULR's residuals in Fig. 1. A departure of JPL's background noise from the white + flicker noise model can also be noted, especially in the vertical component. Instead of a progressive transition

from flicker ($\propto 1/f$) to white (constant power) noise, JPL's Up periodogram rather shows a steady $1/\sqrt{f}$ dependency until about 150 cpy, where it only starts to be dominated by white noise. The reason of this deviation from the white + flicker noise model remains to be investigated.

Many distinct spectral peaks can be observed on top of the background noise of the AC periodograms. For all ACs and components, a broad peak covering both the annual period and the GPS draconitic year (period at which the orientation of the GPS constellation with respect to the Sun repeats, i.e. 351.4 days; Ray et al. 2008) is first present, followed by a second broad peak covering both the semi-annual period and the 2nd harmonic of the GPS draconitic year. Sharper peaks centered on the higher harmonics of the GPS draconitic year are then visible, sometimes up to the 15th harmonic. Those peaks imply the existence of systematic periodic differences between the station position time series of the different ACs, and since the input data used by all ACs are the same for the common stations, these inter-AC differences must be the consequences of analysis specifics. The periodic inter-AC differences at harmonics of the GPS draconitic year are in particular likely related to different modeling of the satellite orbit dynamics.

Three spectral peaks are also common to most ACs and components in the fortnightly band, at periods of 13.7, 14.2, and 14.8 days, which correspond, respectively, to the M_f tide period and to the aliasing periods of the diurnal O_1 and semi-diurnal M_2 tides through daily data processing (Penn and Stewart 2003; Ray et al. 2013a). These peaks are, therefore, likely due to different AC responses to tide modeling errors.

Some spectral peaks can finally be observed for specific ACs and components:

- The three components of COD's and ESA's residuals show distinct peaks at periods of 7.8 and 8.2 days, close to the nominal ground repeat period of GLONASS satellites (8 days). Those peaks are likely related to the use of GLONASS data in COD's and ESA's analyses (Ray et al. 2013a). Their absence from GRG's periodograms is probably due to the fact that GLONASS data are much more weakly weighted than GPS data in GRG's analyses.
- MIT's North residuals show a distinct peak at 7.0 days, for which a possible explanation is the use by MIT of weekly based constraints on their empirical orbit parameters.
- GRG's East and North residuals show unexplained sharp peaks at 13.2 days. Broad peaks can additionally be observed in the three components of GRG's residuals around 3.65 and 2.2 days, which could be caused by date rounding issues within GRG's software.
- GTZ's residuals show clear, unexplained peaks at 16.1 days in the East component and 11.8 days in the North component.

This spectral analysis of the repro2 combination residuals evidences systematic periodic differences between the daily AC station position estimates. However, the daily combination residuals alone (i.e. the differences between the AC station position estimates and their own mean) do not allow a precise understanding of the periodic errors present in the AC (and combined) station position time series. For that purpose, each series of daily AC (and combined) frames should be compared to a long-term linear frame, so as to study the "absolute" non-linear motions present in the AC (and combined) station position time series. This will be the topic of a future study.

2.2 ERP residuals

Figure 3 shows the time series of the AC pole coordinate and pole rate residuals from the daily repro2 combinations, together with their amplitude spectra. Figure 4 similarly shows the time series of the AC LOD residuals, but also the time series of the biases used for the AC LOD calibrations described in Sect. 1.2 (i.e. moving averages of the differences between the AC LOD estimates and the IERS Bulletin A LOD values). AC LOD estimates are related to the observed net nodal rotation of the GNSS constellation, which is in turn directly related to the Earth's dynamic oblateness (Johnson et al. 2001). The long-term drifts in the AC LOD estimates visible in Fig. 4 could, therefore, be related to different modeling of the time variations of the geopotential. Note that larger plots of the AC ERP residual time series are available in Online Resource 1.

Table 4 provides the WRMS of the AC ERP residual time series shown in Figs. 3 and 4, which give an overall indication of the inter-AC level of agreement on ERPs. The WRMS of the AC pole *coordinate* residual time series lie mostly within the 25–40 μas range. The main exception is MIT, with WRMS of 18 and 17 μas for x_p and y_p , respectively (about 1.5 times smaller than the next "best" ACs), and noticeably less scattered residual time series in Fig. 3. There is thus a slight dominance of MIT over the combined pole coordinates. The WRMS of the AC pole *rate* residual time series lie mostly within the 140–200 $\mu\text{as/day}$ range. MIT stands out as an exception again, with WRMS of 79 and 74 μas for \dot{x}_p and \dot{y}_p , respectively, nearly 2 times smaller than the next "best" ACs. MIT thus markedly dominates the combined pole rates. Finally, with the exception of MIT again, the WRMS of the AC LOD residual time series lie within the 8–20 $\mu\text{s/day}$ range. The predominance of MIT over the combined LODs is even more pronounced, with a WRMS of only 2.5 $\mu\text{s/day}$, more than three times smaller than the next "best" ACs.

Let us now discuss the reasons of the predominance of MIT over the combined ERPs. A first key element is that all ACs participating in the combinations have comparable contributions to the combined station positions. The a poste-

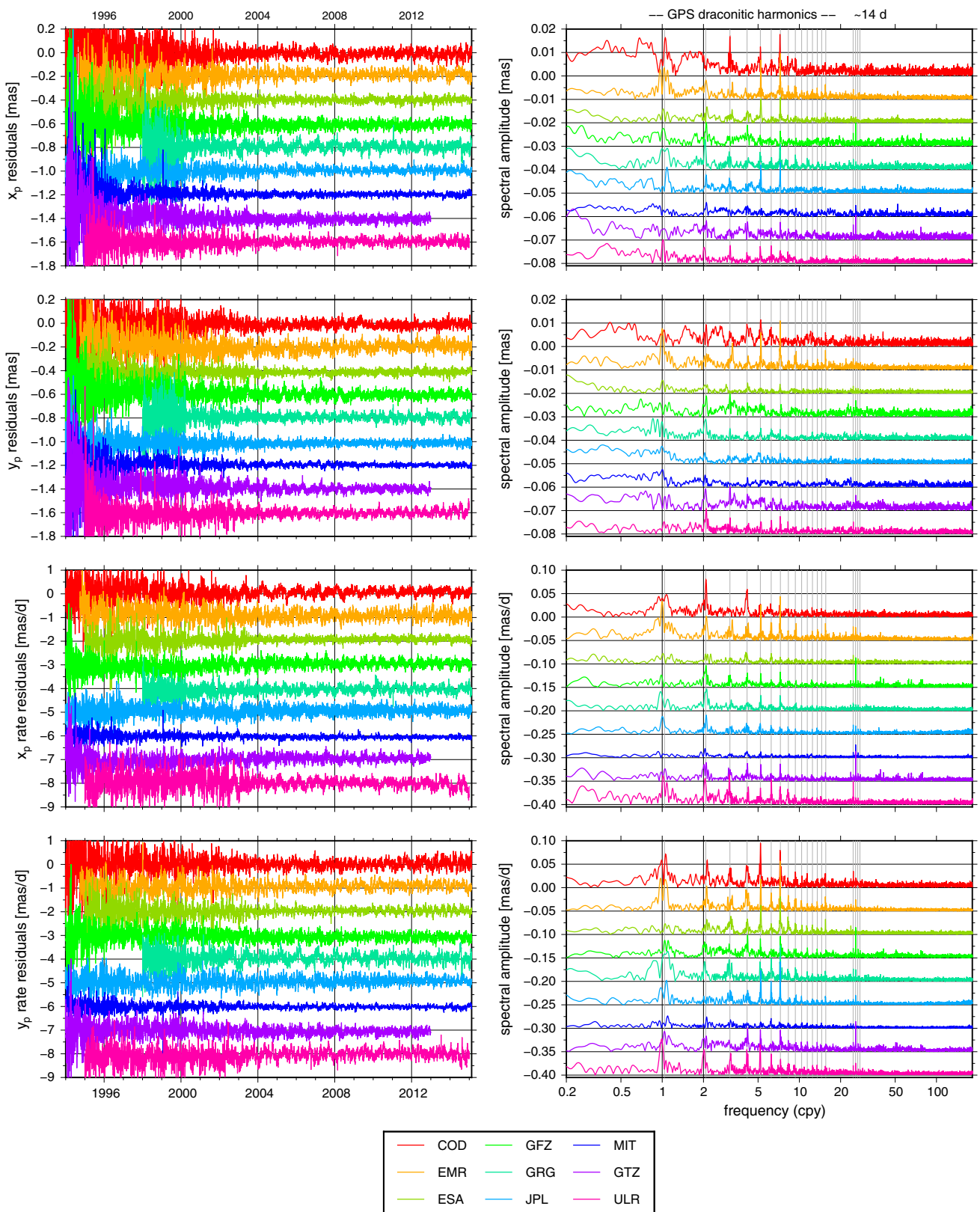


Fig. 3 Left time series of the AC pole coordinate and pole rate residuals from the daily repro2 combinations, offset by multiples of 0.2 mas and 1 mas/day for clarity. Right corresponding amplitude spectra, offset by multiples of 0.01 mas and 0.05 mas/day for clarity. The vertical

black lines indicate the 1 and 2 cpy frequencies. The vertical gray lines indicate the first 15 harmonics of the GPS draconitic year and the 14.8-, 14.2-, 13.7- and 13.2-day periods

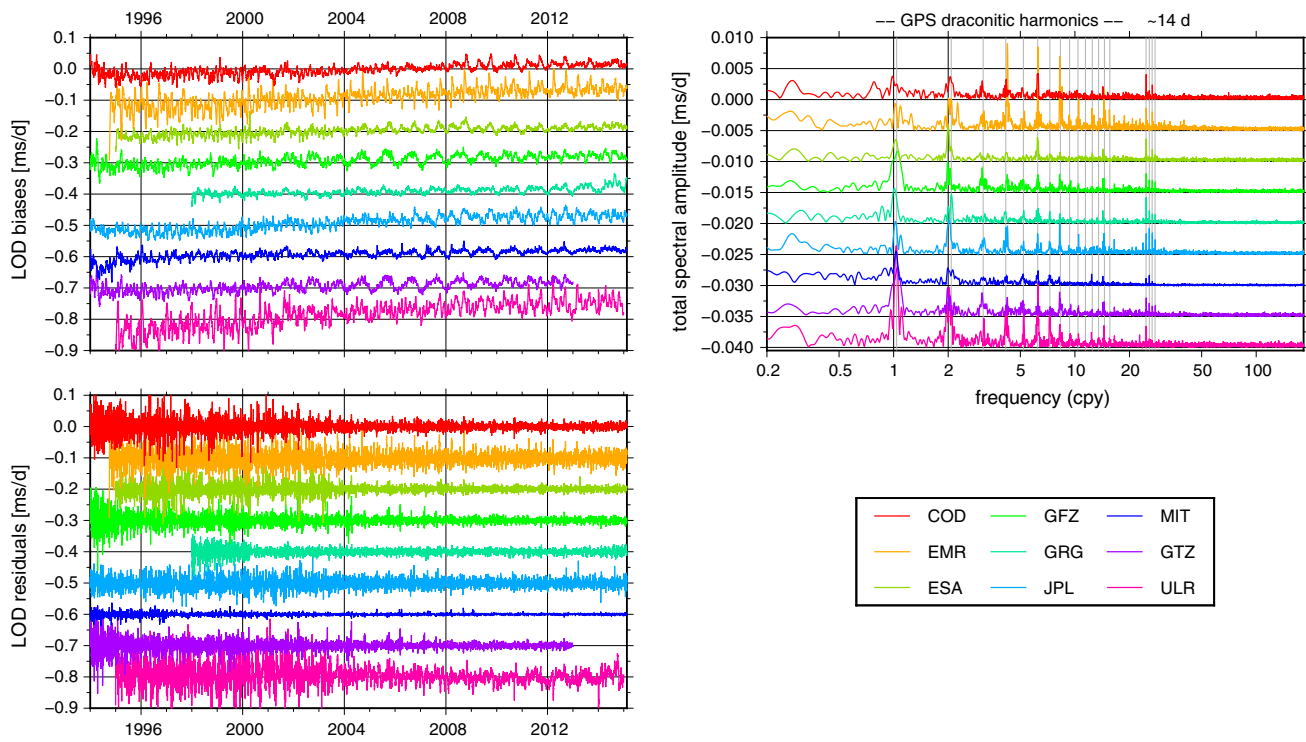


Fig. 4 Bottom left time series of the LOD residuals from the daily repro2 combinations, offset by multiples of 0.1 ms/day for clarity. Top left time series of the biases used for the AC LOD calibrations described in Sect. 1.2, offset by multiples of 0.1 ms/day for clarity. Top right amplitude spectra of the sums of the AC LOD residuals and of the AC LOD

biases, offset by multiples of 0.005 ms/day for clarity. The vertical black lines indicate the 1 and 2 cpy frequencies. The vertical gray lines indicate the first 15 harmonics of the GPS draconitic year and the 14.8-, 14.2-, 13.7- and 13.2-day periods

Table 4 WRMS of the time series of AC ERP residuals from the daily repro2 combinations

	COD	EMR	ESA	GFZ	GRG	JPL	MIT	GTZ	ULR
x_p (μas)	35	39	26	36	36	29	18	28	28
y_p (μas)	33	42	26	38	30	27	17	27	28
\dot{x}_p ($\mu\text{as/day}$)	170	219	131	171	160	166	79	143	181
\dot{y}_p ($\mu\text{as/day}$)	187	186	147	180	203	174	74	148	190
LOD ($\mu\text{s/day}$)	10.2	19.8	9.5	10.7	8.1	14.3	2.5	8.4	20.3

riori variance factors (σ_f^s)² used for the final scaling of the AC covariance matrices are indeed generally close to unity, so that the medians of the 3D station position formal errors remain close to 4 mm in the scaled solutions of all ACs. Another indication of the balance between the AC contributions to the combined station positions is the homogeneity of the unbiased WRMS time series shown in Fig. 1.

Under the assumption that all ACs contribute equally to the combined station positions, the AC contributions to some ERP, for instance LOD, are approximately governed by the ratios $r_{\text{LOD}}^s = \sigma_{\text{LOD}}^s / \bar{\sigma}_{3D}^s$, where σ_{LOD}^s is the formal error of LOD in the solution of AC s and $\bar{\sigma}_{3D}^s$ is the median of the 3D station position formal errors in the solution of AC s . As a matter of fact, the relations between the ratios r_{LOD}^s of the different ACs correspond rather well to the relations between the WRMS of their LOD residual time series. For instance,

during recent years, r_{LOD}^s oscillates around a median value of 0.92 $\mu\text{s/day/mm}$ for ESA and 0.24 $\mu\text{s/day/mm}$ for MIT. The quotient between those two values, 3.8, matches the quotient between the WRMS of ESA's and MIT's LOD residual time series: 9.5 and 2.5 $\mu\text{s/day}$, respectively. Understanding the predominance of MIT over the combined ERPs, therefore, comes down to understanding why the ratios of the ERP formal errors to the station position formal errors are smaller in MIT's solutions.

Part of the explanation resides in the fact that MIT processes large station networks (Fig. 1). Adding more stations into a GNSS solution indeed barely changes the median of the station position formal errors, but has a direct impact on the ERP formal errors, which are approximately inversely proportional to the square root of the number of stations n^s . The large size of MIT's station networks is enough to explain

the slight predominance of MIT over the combined pole coordinates. The products $r_{x_p}^s \times \sqrt{n^s}$ and $r_{y_p}^s \times \sqrt{n^s}$ are indeed of the same order for MIT as for other ACs like ESA and JPL, so that if ESA and JPL had processed as many stations as MIT, they would have contributed as much as MIT to the combined pole coordinates.

The products $r_{\dot{x}_p}^s \times \sqrt{n^s}$, $r_{\dot{y}_p}^s \times \sqrt{n^s}$ and $r_{\text{LOD}}^s \times \sqrt{n^s}$ nevertheless remain smaller for MIT than for any other AC. In other words, the large size of the MIT station networks contributes but is not enough to explain the predominance of MIT over the combined pole rates and LODs. A complementary explanation probably resides in the inter-day constraints applied by MIT to their empirical orbit parameters, which are known to strongly affect the LOD formal errors (T. A. Herring, personal communication).

More generally, it can be concluded that the relative AC contributions to the combined ERPs depend on both the size of the AC station networks (since $r_{ERP}^s \propto 1/\sqrt{n^s}$) and on analysis specifics (since the products $r_{ERP}^s \times \sqrt{n^s}$ show disparities among ACs). A better understanding of those disparities and of their sources would probably be worthwhile for the general purpose of improving GNSS-derived ERPs, but is beyond the scope of the present article.

Like the averaged periodograms of the AC station position residual time series shown in Fig. 2, the amplitude spectra of the AC ERP residual time series shown in Figs. 3 and 4 present many distinct spectral peaks. Spectral peaks at several harmonics of the GPS draconitic year are in particular visible for almost all ACs and ERPs, but generally have disparate amplitudes among ACs for a given ERP and harmonic. Spectral peaks at several fortnightly periods can also be observed in the AC LOD residuals, with AC-dependent amplitudes again. Several AC- and ERP-dependent features can finally be noted, of which we list only the most striking:

- The 14.8- and 14.2-day tidal alias lines clearly appear in GFZ's and GTZ's x_p residuals, while hardly visible in the x_p residuals of the other ACs. Similarly, the 14.2-day line is much more marked in GFZ's and GTZ's pole rate residuals than in those of any other AC.
- Compared to those of all other ACs, EMR's y_p and \dot{x}_p residuals present much higher spectral peaks at several frequencies, including the annual frequency and the 5th and 7th harmonics of the GPS draconitic year. EMR's LOD residuals similarly show particularly high peaks at the even harmonics of the GPS draconitic year from the 4th to the 14th.
- The 14.8-day line is much more marked in ULR's \dot{x}_p residuals than in those of any other AC. ULR's LOD residuals finally show particularly high peaks at the seven first harmonics of the GPS draconitic year.

2.3 Geocenter residuals

Figure 5 shows the time series of the AC geocenter residuals from the daily repro2 combinations, together with their amplitude spectra. Note that, since the geocenter coordinates had been pre-eliminated from ULR's solutions before combination, geocenter residuals were not directly available for ULR. To obtain the time series shown in Fig. 5, ULR's solutions were, therefore, preprocessed again, without pre-eliminating the geocenter coordinates, and compared to the daily repro2 combined solutions. Also note that larger plots of the AC geocenter residual time series are available in Online Resource 1. Table 5 provides the results from linear regressions to the geocenter residual time series shown in Fig. 5. The obtained offsets and rates are of primary importance, since they provide an assessment of the agreement between the origins and origin rates of the long-term frames realized by the daily solutions of each AC. On the other hand, the WRMS values given in Table 5 provide an overall measure of the inter-AC level of agreement on non-linear geocenter motion.

If we except the two ACs that did not contribute to the combined geocenter coordinates (GRG and ULR), the offsets and rates of the AC geocenter residual time series all lie within ± 3 mm and ± 0.3 mm/year, for all three components. There is thus a remarkably good agreement between the long-term behaviors of the origins of the AC frames. GRG and ULR still excepted, the WRMS of the non-linear parts of the AC geocenter residual time series (i.e. the inter-AC level of agreement on non-linear geocenter motion) are mostly around 4 mm for the X and Y components and 8 mm for the Z component. MIT's WRMS, and to a lesser extent GTZ's WRMS, are substantially smaller, indicating that those two ACs dominate the combined geocenter coordinates. This domination, like the predominance of MIT over the combined pole coordinates, seems to be mostly explained by the larger size of the station networks used by these two ACs.

The amplitude spectra of the AC geocenter residual time series shown in Fig. 5 present again spectral peaks at various harmonics of the GPS draconitic year, with AC- and component-dependent amplitudes. The odd harmonics appear particularly clearly in the z_{CM} residual time series of all ACs. COD's z_{CM} residuals show an especially large peak around the 3rd draconitic harmonic, which corresponds to the clear periodic signal visible after 2009, and is likely related to the use of GLONASS data [see Fig. 2 in Meindl et al. (2013)]. The three components of GRG's residuals have the peculiarity of showing high peaks at the annual frequency. Finally, ULR's z_{CM} residuals are clearly outstanding in both the time and frequency domains, which is why ULR did not contribute to the combined geocenter coordinates.

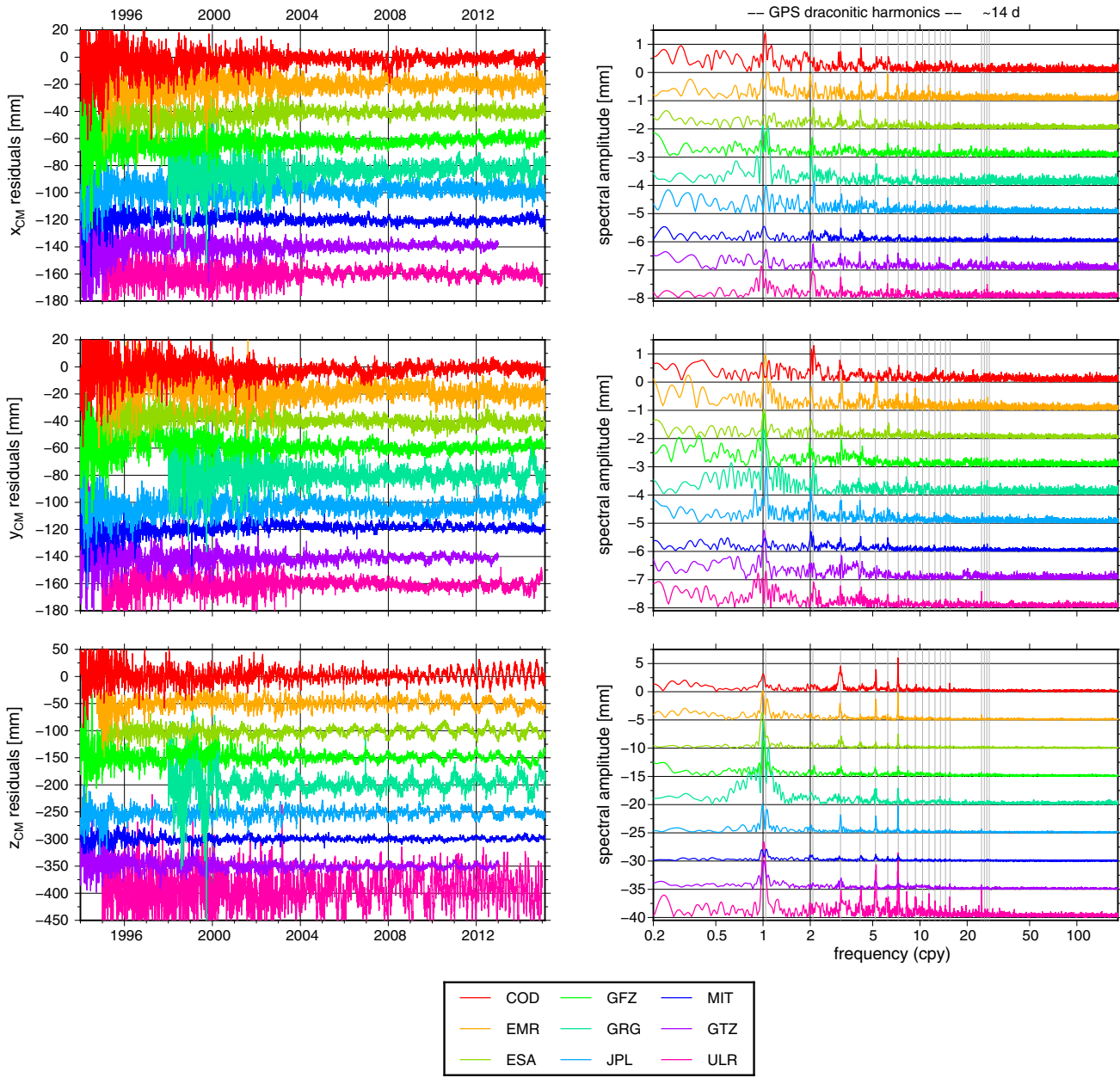


Fig. 5 Left time series of the AC geocenter residuals from the daily repro2 combinations, offset by multiples of 20 mm (x_{CM} and y_{CM}) and 50 mm (z_{CM}) for clarity. Right corresponding amplitude spectra, offset by multiples of 1 mm (x_{CM} and y_{CM}) and 5 mm (z_{CM}) for clarity. The

vertical black lines indicate the 1 and 2 cpy frequencies. The vertical gray lines indicate the first 15 harmonics of the GPS draconitic year and the 14.8-, 14.2-, 13.7- and 13.2-day periods

2.4 Inter-AC scale offsets

As mentioned in Sect. 1.3, no scale offsets were estimated between the AC solutions and the combined solutions during the daily repro2 combinations. The agreement between the scales of the daily AC solutions was nevertheless checked a posteriori. For that purpose, the preprocessed AC solutions were compared to the corresponding daily combined solutions via 7-parameter similarity transformations, using

the inverses of the preprocessed AC covariances matrices as weight matrices. Time series of the estimated scale offsets are represented in Fig. 6, together with their amplitude spectra. The results from linear regressions to the scale offset time series shown in Fig. 6 are provided in Table 6. A larger plot of the same time series is available in Online Resource 1.

With the exception of GRG, the offsets and rates of the AC scale offset time series all lie within ± 0.5 mm and ± 0.05

Table 5 Offsets, rates and WRMS of the residuals obtained from linear regressions to the AC geocenter residual time series from the daily repro2 combinations

	COD	EMR	ESA	GFZ	GRG	JPL	MIT	GTZ	ULR
<i>x</i> _{CM}									
Offset at 2005.0 (mm)	-1.7	-0.2	-1.1	-2.4	-3.9	2.0	0.1	0.7	0.1
Rate (mm/year)	0.07	0.09	0.17	0.22	0.29	0.04	-0.14	0.04	-0.00
WRMS (mm)	3.4	4.6	3.1	3.8	6.0	4.4	2.2	2.6	3.7
<i>y</i> _{CM}									
Offset at 2005.0 (mm)	-2.2	2.3	0.6	1.6	0.8	-2.9	1.7	-1.2	-0.6
Rate (mm/year)	0.10	-0.27	-0.33	-0.19	-0.08	-0.01	0.04	0.09	-0.06
WRMS (mm)	3.5	5.4	3.2	4.3	6.1	4.6	2.2	2.7	3.4
<i>z</i> _{CM}									
Offset at 2005.0 (mm)	0.9	1.8	-1.6	2.0	-0.0	-1.8	0.2	-0.0	7.2
Rate (mm/year)	0.18	-0.17	0.16	-0.31	0.43	0.11	0.06	-0.10	0.20
WRMS (mm)	9.5	8.8	7.1	8.6	12.5	8.0	3.6	5.1	29.1

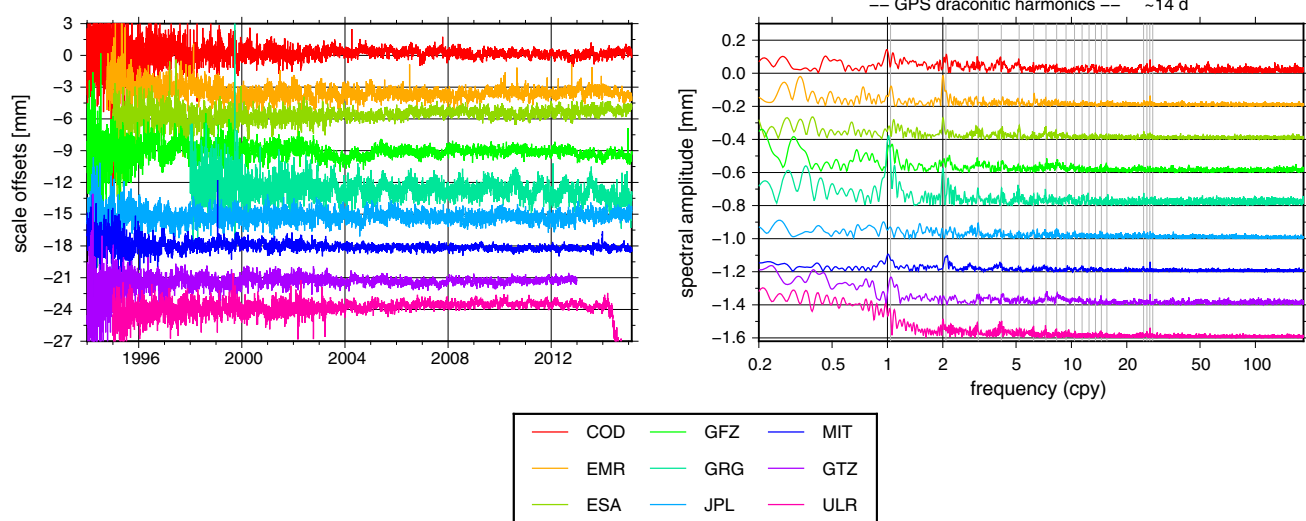


Fig. 6 Left time series of scale offsets estimated between the daily pre-processed AC solutions and the daily repro2 combined solutions, offset by multiples of 3 mm for clarity. Right corresponding amplitude spectra, offset by multiples of 0.2 mm for clarity. The vertical black lines

indicate the 1 and 2 cpy frequencies. The vertical gray lines indicate the first 15 harmonics of the GPS draconitic year and the 14.8-, 14.2-, 13.7- and 13.2-day periods

Table 6 Offsets, rates and WRMS of the residuals obtained from linear regressions to the scale offset time series shown in Fig. 6

	COD	EMR	ESA	GFZ	GRG	JPL	MIT	GTZ	ULR
Offset at 2005.0 (mm)	0.2	-0.5	0.4	-0.1	-0.6	-0.2	-0.1	-0.3	0.3
Rate (mm/year)	-0.01	-0.02	0.04	-0.02	-0.05	0.00	-0.02	0.00	0.03
WRMS (mm)	0.4	0.6	0.5	0.5	0.8	0.5	0.3	0.3	0.4

mm/year. The agreement between the long-term behaviors of the scales of the AC frames is thus excellent. GRG still excepted, the WRMS of the non-linear parts of the AC scale offset time series are of the order of 0.5 mm. Moreover, the amplitude spectra of the AC scale offset time series hardly show traces of spurious spectral peaks. This excellent agreement between the scales of the AC frames justifies a posteriori our choice not to estimate AC scale offsets during the daily repro2 combinations. Let us recall that the purpose of this

choice was to avoid alignments in scale of the daily repro2 solutions to some reference frame, which would have caused aliasing of the non-linear station motions (Sect. 1.3).

GRG's scale offset time series has the peculiarity of showing a pronounced peak at the annual frequency. Finally, ULR's scale offsets progressively diverge during year 2014 because of a software update issue, which is why zero weights were assigned to ULR's solutions in the daily combinations of year 2014.

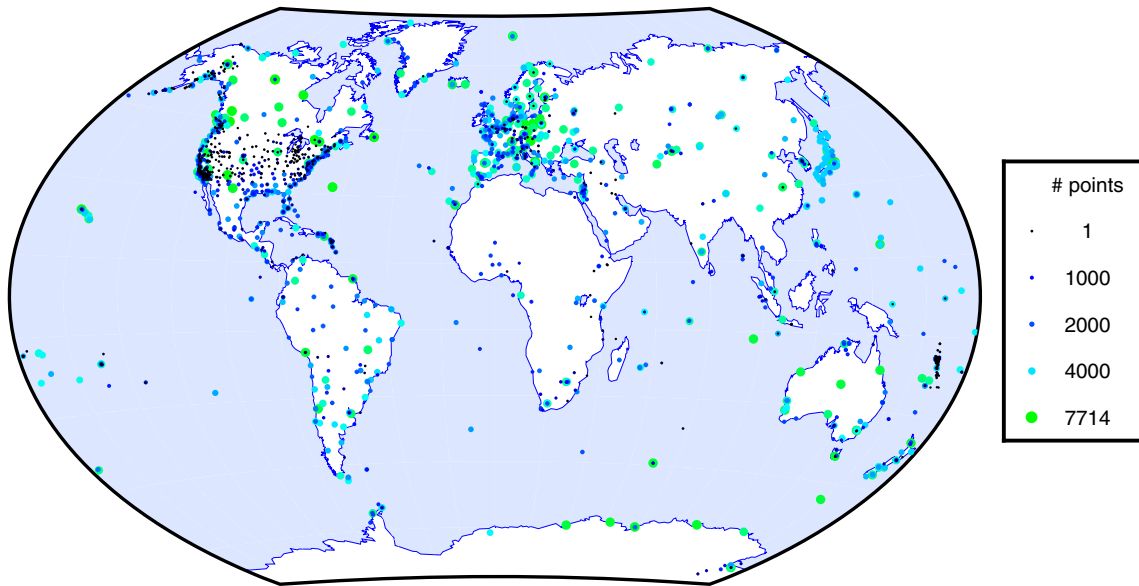


Fig. 7 Map of the stations present in the daily repro2 combined solutions. The size and color of each dot is function of the number of points (days) in the repro2 position time series of each station

3 Some aspects of the repro2 combined dataset

It is beyond the scope of this article to provide an extensive evaluation of the accuracy of the repro2 combined products. Evaluating the accuracy of the repro2 combined station position time series would indeed require a dedicated study involving a complete modeling of their signal and noise contents. It can nevertheless be mentioned here that the residuals from a preliminary long-term stacking of the daily repro2 combined solutions performed in the frame of the ITRF2014 analysis have WRMS of about 2 mm in horizontal and 5 mm in vertical, but exhibit clear spectral peaks at harmonics of the GPS draconitic year and several fortnightly periods (Altamimi et al. 2015). The task of evaluating the accuracy of the repro2 combined ERPs is also made difficult by the lack of external reference with sufficient accuracy and will, therefore, not be attempted here. For reference purpose, we nevertheless deem it useful to address particular aspects of the repro2 combined dataset in the present article.

Section 3.1 thus provides basic facts about the network of stations present in the daily repro2 combined solutions. Sections 3.2 and 3.3 then provide succinct evaluations of the repro2 combined geocenter coordinate time series and of the scale of the daily repro2 combined solutions.

3.1 Station network

The overall set of daily repro2 combined solutions comprises a total of 1845 different stations of which the distribution is shown in Fig. 7. As can be seen in Fig. 8, all stations are far from being present in the 7714 daily repro2 combined

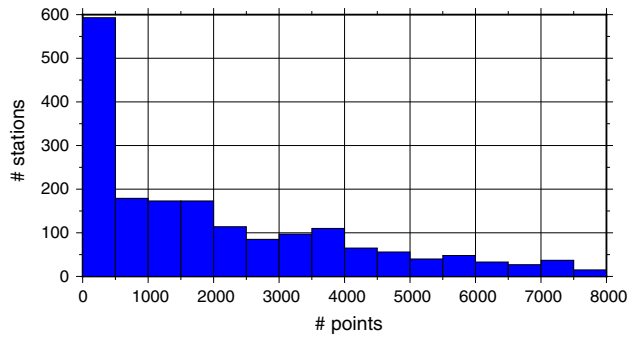


Fig. 8 Histogram of the numbers of points (days) in the repro2 station position time series

solutions, and stations with short time series are actually over-represented. Only 58 % (1073) of the 1845 stations indeed have position time series with more than 1000 points, and 17 % (321) have series with more than 4000 points. A significant fraction of the repro2 station position time series are, therefore, not suitable for reliable velocity estimation, hence for contributing to the ITRF2014.

Only 31 % (578) of the 1845 stations are or have been part of the IGS network. Most the remaining stations are part of either regional (EPN, SIRGAS...), national (CORS, ARGN...) or geophysically-oriented (PBO, SONEL...) permanent GNSS networks. To fill in the metadata blocks of the daily repro2 combined SINEX files, site logs were gathered from different sources of which a list can be found in the combination summaries. Site logs could thus be attributed to 91 % (1683) of the 1845 stations. For the remaining 162 stations, the metadata provided in the repro2 combined SINEX

files rely on those given in the AC SINEX files. Some non-IGS stations present in the combined repro2 dataset may not meet the IGS site guidelines ensuring the high quality and stability of the IGS tracking stations and should, therefore, be handled with care.

3.2 Geocenter coordinates

The geocenter coordinates x_{CM}^c provided in the daily repro2 combined SINEX files represent the coordinates of CM, as observed by the average of the contributing ACs, in the IGB08 reference frame. The IGB08 reference frame inherits the origin of ITRF2008, which linearly follows CM, as sensed by SLR (Altamimi et al. 2011). The offsets and rates of the repro2 combined geocenter coordinate time series provided in Table 7, therefore, correspond to the long-term drift between CM as observed by the average of the repro2 ACs and CM as sensed by SLR. Except a 7 mm offset in the Z component, they are of the order of a few mm and a few tenths of mm/year, i.e. within the estimated uncertainties of the origin and origin rate of ITRF2008 (Altamimi et al. 2011; Wu et al. 2011; Argus 2012; Collilieux et al. 2014).

Furthermore, the non-linear parts of the repro2 combined geocenter coordinate time series correspond to the non-linear geocenter motion observed by the average of the repro2 ACs. They are compared in Fig. 9 with non-linear geocenter motion time series derived from the SLR contribution to ITRF2014. As geophysically expected, the spectra of the SLR-derived time series show no other peaks than annual peaks (and small semi-annual peaks in the X and Z components). On the other hand, the spectra of the repro2 geocenter time series show a number of peaks at harmonics of the GPS draconitic year. The X component mainly presents a broad peak centered around the 3rd draconitic harmonic. The Y component additionally shows distinct peaks at the 4th, 6th and 8th harmonics. Finally, the Z component presents clear peaks at all harmonics from the 2nd to the 7th.

Table 7 Offsets, rates, amplitudes, phases and WRMS of the residuals obtained from regressions of linear trends plus annual signals to the daily repro2 combined geocenter coordinate time series

	x_{CM}	y_{CM}	z_{CM}
Offset (mm)	1.6	2.6	7.0
Rate (mm/year)	0.28	-0.40	-0.18
Amplitude (mm)	1.5 (2.6)	3.6 (2.9)	3.8 (6.1)
Phase (°)	41 (50)	310 (321)	181 (25)
WRMS (mm)	3.6	3.5	6.5

Offsets are given at epoch 2005.0 and phases according to the model $A \cos(2\pi(t - 2005.0) - \phi)$. The parenthesized amplitudes and phases were derived from similar regressions to geocenter coordinate time series derived from the SLR contribution to ITRF2014

The annual and longer periods of both the SLR-derived and repro2 geocenter time series are highlighted by the solid lines in the left part of Fig. 9. Amplitudes and phases of the annual signals contained in the series are additionally given in Table 7. In the X and Y components, a good agreement in phase can be observed between the annual signals of both series. The amplitude of the annual signal present in the repro2 time series, however, clearly varies with time, and is globally underestimated in the X component and overestimated in the Y component, compared to SLR. On the other hand, the near-annual signal present in the Z component of the repro2 time series is mostly out-of-phase with SLR and shows again clear amplitude variations. This behavior of the near-annual signals present in the repro2 time series could be the result of alternatively constructive and destructive interferences between real geocenter motion and periodic errors at the fundamental GPS draconitic frequency.

3.3 Terrestrial scale

To investigate the time evolution of the scale of the daily repro2 combined solutions, we compared them to the IGB08 reference frame via 7-parameter similarity transformations, using the inverses of the daily combined covariance matrices as weight matrices. The time series of the estimated scale offsets is represented in Fig. 10, together with its amplitude spectrum.

An offset, estimated to -1.5 mm at epoch 2005.0, can first be noticed between the scale of the daily repro2 combined solutions and the scale of IGB08, which is inherited from the ITRF2008 scale. The mean scale of the daily repro2 combined solutions is conventionally determined by the igs08.atx values adopted for satellite PCOs (Zhu et al. 2003; Ray et al. 2013b). Those had been derived based on AC solutions from the repro1 campaign so as to give access to the ITRF2008 scale (Reischburg et al. 2012). The observed scale offset is, therefore, likely due to modeling changes from the repro1 to the repro2 campaign, and can actually mostly be explained by the introduction of Earth radiation pressure modeling and antenna thrust into the repro2 standards (Rodriguez-Solano et al. 2011b).

The scale rate of the daily repro2 combined solutions is governed by the assumption that satellite PCOs remain constant with time, and shows a difference of -0.03 mm/year with the IGB08/ITRF2008 scale rate. According to the study conducted by Collilieux and Schmid (2012) on AC solutions from the repro1 campaign, the PCO time invariability assumption is only met at a level of 5 mm/year, hence allowing a determination of the terrestrial scale rate with a precision of about 0.25 mm/year. The scale rate difference between the daily repro2 combined solutions and IGB08/ITRF2008 can, therefore, not be considered significant. It can merely be concluded that the PCO time invariability assumption gives

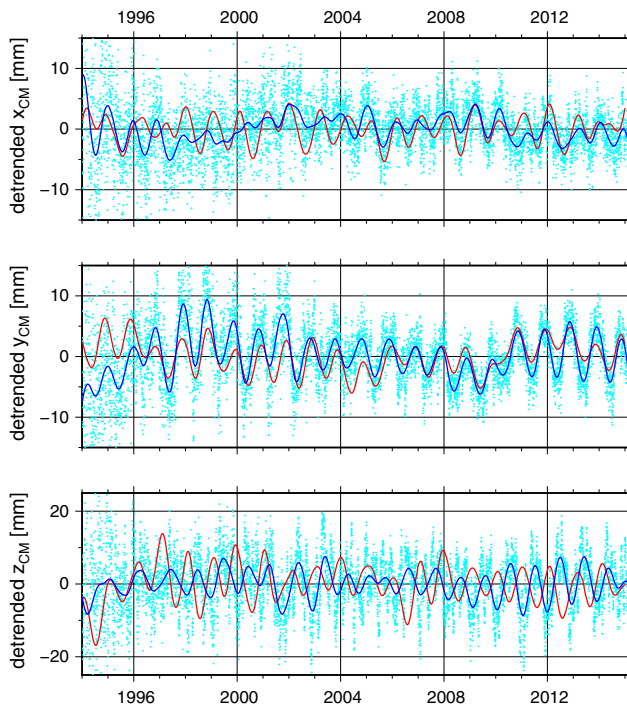
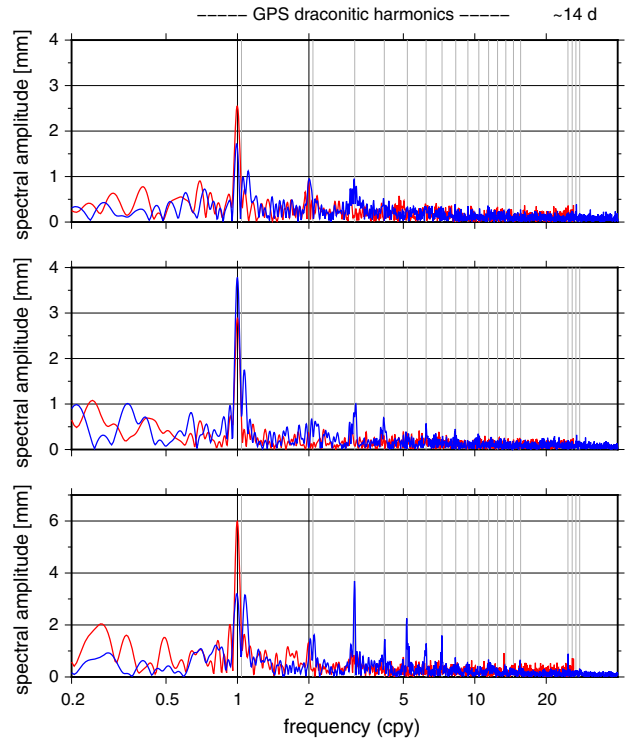


Fig. 9 Left, cyan dots detrended time series of daily repro2 combined geocenter coordinates. Left, blue lines same time series smoothed by a Vondrák filter with a 1.25 cpy cutoff frequency. Left, red lines similarly detrended and smoothed time series of geocenter coordinates derived



from the SLR contribution to ITRF2014. Right, blue lines amplitude spectra of the repro2 combined geocenter coordinate time series. Right, red lines amplitude spectra of geocenter coordinate time series derived from the SLR contribution to ITRF2014

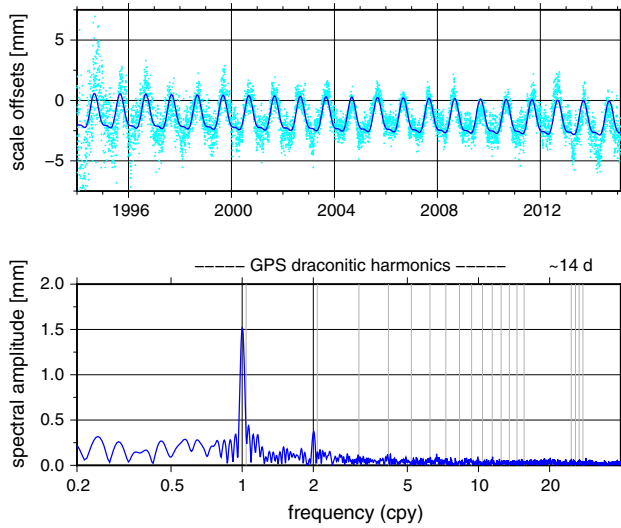


Fig. 10 Top, cyan dots time series of scale offsets estimated between the daily repro2 combined solutions and IGb08. Top, blue line result from the regression of a linear trend, an annual signal and a semi-annual signal to the scale offset time series. Bottom amplitude spectrum of the scale offset time series

access to the IGb08/ITRF2008 scale rate within its own precision level.

Finally, the non-linear scale differences between the daily repro2 combined solutions and IGb08 are expected to result

from the aliasing of non-linear deformations of the station network into the estimated daily scale offsets. As can be seen in Fig. 10, they are almost exclusively composed of annual and semi-annual terms and show no trace of spurious spectral peaks. This tends to indicate that the non-linear variations of the net height of the repro2 station network are reliably determined, as also suggested by the excellent agreement between the scales of the daily AC frames (Sect. 2.4).

However, part of the non-linear scale differences between the daily repro2 combined solutions and IGb08 could also stem from imperfect igs08.atx satellite PCO values combined with changes in the observed satellite constellation (Ge et al. 2005). In particular, igs08.atx contains preliminary PCO values for the satellites launched since October 2012, i.e. up to 6 GPS and 5 GLONASS satellites at the end of the repro2 period. The contribution of the igs08.atx satellite PCO errors to the observed non-linear scale differences is hardly assessable for the time being. But a reassessment of the satellite PCOs based on the repro2 AC solutions is planned in view of the preparation of an updated set of antenna calibrations (igs14.atx). Studying the impact of the igs08.atx → igs14.atx satellite PCO updates on the scale of the daily repro2 solutions could then shed some light on that question.

4 Summary

Based on the contributions from nine ACs, a homogeneous series of more than 21 years of daily combined terrestrial frame solutions including station positions, ERPs and geocenter coordinates has been derived and constitutes the IGS contribution to ITRF2014.

The analysis of the combination residuals reveals that the participating ACs have comparable contributions to the combined station positions. After 2004, once the AC GPS station networks reach maturity, the global inter-AC level of agreement on station positions remains around 1.5 mm in the horizontal components and 4 mm in the vertical component. A spectral analysis of the combination residuals reveals systematic periodic differences between the station position time series of the different ACs, mainly at harmonics of the GPS draconitic year and at several fortnightly periods. A few AC-specific features can finally be noted, some of which are explained by known analysis details, while others remain under investigation.

The global inter-AC level of agreement on ERPs is about 25–40 μas for pole coordinates, 140–200 $\mu\text{as}/\text{day}$ for pole rates and 8–20 $\mu\text{s}/\text{day}$ for calibrated LOD estimates. The repro2 combined ERPs (especially pole rates and LOD) are dominated by MIT's contribution, likely due to both the large size of MIT's station networks and the application by MIT of inter-day constraints on their empirical orbit parameters.

The offsets and rates of the geocenter residual time series from the contributing ACs lie within ± 3 mm and ± 0.3 mm/year, indicating a rather good agreement between the long-term behaviors of the origins of the AC frames. On the other hand, the inter-AC level of agreement on non-linear geocenter motion is only around 4 mm for the X and Y components and 8 mm for the Z component, and large periodic inter-AC differences at several harmonics of the GPS draconitic year can be noticed, especially for the Z component of geocenter motion.

The long-term agreement between the scales of the contributing AC frames is excellent, with offsets and rates below 0.5 mm and 0.05 mm/year. The non-linear inter-AC scale differences are also of the order of 0.5 mm and hardly show any trace of spurious spectral peaks.

The numbers given above are indications of the internal precision of the AC repro2 products. The precision of the combined products should benefit from the number of ACs being combined to reach a lower level, to the extent that the AC errors are uncorrelated with each other. The results from the daily repro2 combinations do, however, not allow an evaluation of the absolute accuracy of the repro2 combined products. Evaluating the accuracy of the repro2 combined station position time series would require a dedicated study involving a complete modeling of their signal and noise contents, and the task of evalu-

ating the accuracy of the repro2 combined ERPs is made difficult by the lack of external reference with sufficient accuracy. We, therefore, limited ourselves to succinct evaluations of the repro2 combined geocenter coordinate time series and of the scale of the repro2 combined terrestrial frames.

Except a 7 mm offset in the Z component, the offsets and rates of the repro2 combined geocenter coordinate time series are of the order of a few mm and a few mm/year, i.e. within the estimated uncertainties of the origin and origin rate of ITRF2008. The annual part of the repro2 combined geocenter coordinate time series, however, shows a limited (for the X and Y components) to poor (for the Z component) agreement with SLR-derived geocenter time series.

The mean scale of the repro2 combined terrestrial frames is offset from the ITRF2008 scale by -1.5 mm at epoch 2005.0, likely due to modeling changes from the repro1 to the repro2 campaign. The estimated scale rate between the repro2 combined terrestrial frames and ITRF2008 is -0.03 mm/year, which is not significant given the precision with which the PCO time invariability assumption allows an intrinsic GNSS scale rate determination. Finally, the non-linear scale variations between the daily repro2 combined solutions and IGb08 seem reliable. A further study of the impact of possible imperfections in the igs08.atx satellite PCO values on those non-linear scale variations is, however, needed.

Acknowledgments We thank all participating Analysis Centers for the huge efforts they invested into the second IGS reprocessing campaign.

References

- Altamimi Z, Collilieux X, Legrand J, Garayt B, Boucher C (2007) ITRF2005: a new release of the International Terrestrial Reference Frame based on time series of station positions and Earth Orientation Parameters. *J Geophys Res* 112(B9). doi:[10.1029/2007JB004949](https://doi.org/10.1029/2007JB004949)
- Altamimi Z, Collilieux X, Métivier L (2011) ITRF2008: an improved solution of the International Terrestrial Reference Frame. *J Geod* 85(8):457–473. doi:[10.1007/s00190-011-0444-4](https://doi.org/10.1007/s00190-011-0444-4)
- Altamimi Z, Collilieux X, Rebischung P, Métivier L (2015) 1985–2015: thirty years of R&D on the International Terrestrial Reference Frame. In: Abstract presented at IUGG general assembly, Prague
- Argus DF (2012) Uncertainty in the velocity between the mass center and surface of Earth. *J Geophys Res* 117(B10). doi:[10.1029/2012JB009196](https://doi.org/10.1029/2012JB009196)
- Collilieux X, Schmid R (2012) Evaluation of the ITRF2008 GPS vertical velocities using satellite antenna z-offsets. *GPS Solut* 17(2):237–246. doi:[10.1007/s10291-012-0274-8](https://doi.org/10.1007/s10291-012-0274-8)
- Collilieux X, Métivier L, Altamimi Z, van Dam T, Ray J (2011) Quality assessment of GPS reprocessed terrestrial reference frame. *GPS Solut* 15(3):219–231. doi:[10.1007/s10291-010-0184-6](https://doi.org/10.1007/s10291-010-0184-6)
- Collilieux X, van Dam T, Ray J, Coulot D, Métivier L, Altamimi Z (2012) Strategies to mitigate aliasing of loading signals while esti-

- mating GPS frame parameters. *J Geod* 86(1):1–14. doi:[10.1007/s00190-011-0487-6](https://doi.org/10.1007/s00190-011-0487-6)
- Collilieux X, Altamimi Z, Argus DF, Boucher C, Dermanis A, Haines BJ, Herring TA, Kreemer CW, Lemoine FG, Ma C, MacMillan DS, Mäkinen J, Métivier L, Ries J, Teferle FN, Wu X (2014) External evaluation of the Terrestrial Reference Frame: report of the task force of the IAG sub-commission 1.2. In: Rizos C, Willis P (eds) Proceedings of the XXV IUGG general assembly. IAG Symp, vol 139. Springer, Berlin, pp 197–202. doi:[10.1007/978-3-642-37222-3_25](https://doi.org/10.1007/978-3-642-37222-3_25)
- Dilssner F (2010) GPS IIF-1 satellite antenna phase center and attitude modeling. Inside GNSS 5(6):59–64
- Dilssner F, Springer T, Gienger G, Dow J (2011) The GLONASS-M satellite yaw-attitude model. *Adv Space Res* 47(1):160–171. doi:[10.1016/j.asr.2010.09.007](https://doi.org/10.1016/j.asr.2010.09.007)
- Dow JM, Neilan RE, Rizos C (2009) The international GNSS service in a changing landscape of global navigation satellite systems. *J Geod* 83(3–4):191–198. doi:[10.1007/s00190-008-0300-3](https://doi.org/10.1007/s00190-008-0300-3)
- Ferland R, Kouba J, Hutchison D (2000) Analysis methodology and recent results of the IGS network combination. *Earth Planets Space* 52(1):953–957. doi:[10.1186/BF03352311](https://doi.org/10.1186/BF03352311)
- Ge M, Gendt G, Dick G, Zhang FP, Reigber C (2005) Impact of GPS satellite antenna offsets on scale changes in global network solutions. *Geophys Res Lett* 32(6). doi:[10.1029/2004GL022224](https://doi.org/10.1029/2004GL022224)
- Griffiths J, Choi K (2013) Analysis center coordinator report. In: Dach R, Jean Y (eds) International GNSS service technical report 2012. Astronomical Institute, University of Bern, pp 21–34
- Johnson TJ, Kammeyer P, Ray J (2001) The effects of geophysical fluids on motions of the global positioning system satellites. *Geophys Res Lett* 28(17):3329–3332. doi:[10.1029/2001GL013180](https://doi.org/10.1029/2001GL013180)
- Kouba J (2009) A simplified yaw-attitude model for eclipsing GPS satellites. *GPS Solut* 13(1):1–12. doi:[10.1007/s10291-008-0092-1](https://doi.org/10.1007/s10291-008-0092-1)
- Meindl M, Beutler G, Thaller D, Dach R, Jäggi A (2013) Geocenter coordinates estimated from GNSS data as viewed by perturbation theory. *Adv Space Res* 51(7):1047–1064. doi:[10.1016/j.asr.2012.10.026](https://doi.org/10.1016/j.asr.2012.10.026)
- Penna NT, Stewart MP (2003) Aliased tidal signatures in continuous GPS height time series. *Geophys Res Lett* 30(23):2184. doi:[10.1029/2003GL018828](https://doi.org/10.1029/2003GL018828)
- Petit G, Luzum B, IERS Conventions (2010) IERS technical note 36. Verlag des Bundesamts für Kartographie und Geodäsie, Frankfurt am Main
- Press W, Teukolsky S, Vetterling W, Flannery B (1996) Numerical recipes in C. Cambridge University Press, Cambridge
- Ray JR (1996) Measurements of length of day using the global positioning system. *J Geophys Res* 101(B9):20,141–20,149. doi:[10.1029/96JB01889](https://doi.org/10.1029/96JB01889)
- Ray JR (2009) A quasi-optimal, consistent approach for combination of UT1 and LOD. In: Drewes H (ed) Geodetic reference frames. IAG Symp, vol 134. Springer, Berlin, pp 239–243. doi:[10.1007/978-3-642-00860-3_37](https://doi.org/10.1007/978-3-642-00860-3_37)
- Ray J, Altamimi Z, Collilieux X, van Dam T (2008) Anomalous harmonics in the spectra of GPS position estimates. *GPS Solut* 12(1):55–64. doi:[10.1007/s10291-007-0067-7](https://doi.org/10.1007/s10291-007-0067-7)
- Ray J, Griffiths J, Collilieux X, Rebischung P (2013a) Subseasonal GNSS positioning errors. *Geophys Res Lett* 40(22):5854–5860. doi:[10.1002/2013GL058160](https://doi.org/10.1002/2013GL058160)
- Ray JR, Rebischung P, Schmid R (2013b) Dependence of IGS products on the ITRF datum. In: Altamimi Z, Collilieux X (eds) Reference frames for applications in geosciences. IAG Symp, vol 138. Springer, Berlin, pp 63–67. doi:[10.1007/978-3-642-32998-2_11](https://doi.org/10.1007/978-3-642-32998-2_11)
- Rebischung P (2014) Can GNSS contribute to improving the ITRF definition? PhD thesis, Ecole Doctorale Astronomie et Astrophysique d'Ile-de-France. http://recherche.ign.fr/theses_2014/TheseIGN2014_LAREG_Rebischung.pdf. Accessed 5 Apr 2016
- Rebischung P, Garayt B (2013) Recent results from the IGS terrestrial frame combinations. In: Altamimi Z, Collilieux X (eds) Reference frames for applications in geosciences. IAG Symp, vol 138. Springer, Berlin, pp 69–74. doi:[10.1007/978-3-642-32998-2_12](https://doi.org/10.1007/978-3-642-32998-2_12)
- Rebischung P, Griffiths J, Ray J, Schmid R, Collilieux X, Garayt B (2012) IGS08: the IGS realization of ITRF2008. *GPS Solut* 16(4):483–494. doi:[10.1007/s10291-011-0248-2](https://doi.org/10.1007/s10291-011-0248-2)
- Rebischung P, Garayt B, Collilieux X, Altamimi Z (2013) IGS reference frame working group coordinator report. In: Dach R, Jean Y (eds) International GNSS service technical report 2012. Astronomical Institute, University of Bern, pp 171–178
- Rebischung P, Altamimi Z, Springer T (2014) A collinearity diagnosis of the GNSS geocenter determination. *J Geod* 88(1):65–85. doi:[10.1007/s00190-013-0669-5](https://doi.org/10.1007/s00190-013-0669-5)
- Rodriguez-Solano C, Hugentobler U, Steigenberger P (2011a) Earth radiation pressure model for GNSS satellites. In: Abstract EGU2011-9824 presented at EGU general assembly, Vienna
- Rodriguez-Solano CJ, Hugentobler U, Steigenberger P, Lutz S (2011b) Impact of earth radiation pressure on GPS position estimates. *J Geod* 86(5):309–317. doi:[10.1007/s00190-011-0517-4](https://doi.org/10.1007/s00190-011-0517-4)
- Scargle J (1982) Studies in astronomical time series analysis. II—statistical aspects of spectral analysis of unevenly spaced data. *Astrophys J* 263:835–853. doi:[10.1086/160554](https://doi.org/10.1086/160554)
- Sillard P (1999) Modélisation des systèmes de référence terrestres. PhD thesis, Observatoire de Paris
- Steigenberger P, Rothacher M, Dietrich R, Fritsche M, Rülke A, Vey S (2006) Reprocessing of a global GPS network. *J Geophys Res* 111(B5). doi:[10.1029/2005JB003747](https://doi.org/10.1029/2005JB003747)
- Steigenberger P, Rothacher M, Fritsche M, Rülke A, Dietrich R (2009) Quality of reprocessed GPS satellite orbits. *J Geod* 83(3–4):241–248. doi:[10.1007/s00190-008-0228-7](https://doi.org/10.1007/s00190-008-0228-7)
- Vondrák J (1969) A contribution to the problem of smoothing observational data. *B Astron I Czech* 20(6):349–355
- Vondrák J (1977) Problem of smoothing observational data II. *B Astron I Czech* 28(2):84–89
- Wu X, Collilieux X, Altamimi Z, Vermeersen BLA, Gross RS, Fukumori I (2011) Accuracy of the International Terrestrial Reference Frame origin and earth expansion. *Geophys Res Lett* 38(13):L13,304. doi:[10.1029/2011GL047450](https://doi.org/10.1029/2011GL047450)
- Zhu SY, Massmann FH, Yu Y, Reigber C (2003) Satellite antenna phase center offsets and scale errors in GPS solutions. *J Geod* 76(11–12):668–672. doi:[10.1007/s00190-002-0294-1](https://doi.org/10.1007/s00190-002-0294-1)